

Molecular dynamics simulation, *ab initio* calculation, and size-selected anion photoelectron spectroscopy study of initial hydration processes of calcium chloride

Zhili He,^{1,a)} Gang Feng,^{2,3,a)} Bin Yang,^{2,4} Lijiang Yang,¹ Cheng-Wen Liu,^{1,5}

Hong-Guang Xu,^{2,4} Xi-Ling Xu,^{2,4} Wei-Jun Zheng,^{2,4,b)} and Yi Qin Gao^{1,b)}

¹Beijing National Laboratory for Molecular Sciences, College of Chemistry and Molecular Engineering, Peking University, Beijing 100871, China

²Beijing National Laboratory for Molecular Sciences, State Key Laboratory of Molecular Reaction Dynamics, Institute of Chemistry, Chinese Academy of Sciences, Beijing 100190, China

³School of Chemistry and Chemical Engineering, Chongqing University, Chongqing 401331, China

⁴University of Chinese Academy of Sciences, Beijing 100049, China

⁵Department of Biomedical Engineering, The University of Texas at Austin, Austin, Texas 78712, USA

(Received 31 January 2018; accepted 9 May 2018; published online 30 May 2018)

To understand the initial hydration processes of CaCl_2 , we performed molecular simulations employing the force field based on the theory of electronic continuum correction with rescaling. Integrated tempering sampling molecular dynamics were combined with *ab initio* calculations to overcome the sampling challenge in cluster structure search and refinement. The calculated vertical detachment energies of $\text{CaCl}_2(\text{H}_2\text{O})_n^-$ ($n = 0-8$) were compared with the values obtained from photoelectron spectra, and consistency was found between the experiment and computation. Separation of the Cl—Ca ion pair is investigated in $\text{CaCl}_2(\text{H}_2\text{O})_n^-$ anions, where the first Ca—Cl ionic bond required 4 water molecules, and both Ca—Cl bonds are broken when the number of water molecules is larger than 7. For neutral $\text{CaCl}_2(\text{H}_2\text{O})_n$ clusters, breaking of the first Ca—Cl bond starts at $n = 5$, and 8 water molecules are not enough to separate the two ion pairs. Comparing with the observations on magnesium chloride, it shows that separating one ion pair in $\text{CaCl}_2(\text{H}_2\text{O})_n$ requires fewer water molecules than those for $\text{MgCl}_2(\text{H}_2\text{O})_n$. Coincidentally, the solubility of calcium chloride is higher than that of magnesium chloride in bulk solutions. *Published by AIP Publishing.* <https://doi.org/10.1063/1.5024279>

I. INTRODUCTION

The salt effects of the Hofmeister series affect chemical and biological systems in many ways.¹⁻³ For example, dynamical properties of both water and water/air surface tension are influenced by salts.⁴⁻⁶ Although salts play diverse roles in many different and complex systems, functions of salts need to be understood in a more fundamental way of water-ion interaction. Dissolution of salts is a fundamental process in chemistry to understand water-ion interaction, and many efforts have been made to study the solvation process of salts in water both experimentally and theoretically.⁷⁻¹⁶ Measuring solubility of salts in bulk can be readily done, but investigation of ion-ion and ion-water interactions on a molecular level is difficult. Salt-water clusters serve as an important model system to investigate water-ion interaction at the atomic level,¹⁷⁻²⁰ including the water molecule arrangement in the first solvation shell and the ion pair evolution.

Ions have two typical structures, solvent-separated ion pairs (SSIPs) and contact ion pairs (CIPs). In forming SSIPs, the anion and cation are separated by the solvent molecules. Otherwise, the anion and cation interact with each other

directly through electrostatic interaction without interference from solvents and form CIPs. In some bulk solution studies, solvent-separated ion pairs (SSIPs) and solvent-shared (SIPs) can be distinguished. However, in clusters within ten water molecules, the concept of SSIPs and SIPs is the same or not differentiated too much, due to the limited number of water molecules. Furthermore, we emphasized the separation of ion pairing by water, and the concept and term of sharing is not mentioned in this study. So we use CIPs and SSIPs here also for being consistent with the previous studies.^{21,22} Solvent molecules can significantly affect the ionic bond of salts, so the electronic state of a CIP would be different from that of a SSIP. Therefore, one interesting question is to see how many water molecules are needed to separate ionic pairs.²³

A reliable approach for studying the evolution of CIP to SSIP structures in solvation is to probe the change of salt electronic state with the increasing number of solvent molecules using anion photoelectron spectroscopy combined with theoretical calculations. Alkali halides have been extensively studied using this approach; for example, microsolvation processes in the first stage of LiI and CsI dissolution have been investigated by using photoelectron spectroscopy and *ab initio* calculations.²² Step by step emergence of SSIP of the NaCl ion pair was observed in salt water clusters, and the energy degeneration of cluster structures in $\text{NaCl}(\text{H}_2\text{O})_n$ implies the

^{a)}Z. He and G. Feng contributed equally to this work.

^{b)}Electronic addresses: zhengwj@iccas.ac.cn and gaoyq@pku.edu.cn

coexistence of CIP and SSIP in saturated NaCl solution.²⁵ Nevertheless, alkaline earth metal halides are not well-studied, one of the reasons is the difficulties of their accurate force field description.

Calcium chloride is extensively used in industry, agriculture, nutrition, and medicine. For example, calcium chloride is the major ingredient of construction and building materials²⁶ and deicing agents.²⁷ In polymer science, calcium chloride affects electro dialysis²⁸ and functions of microencapsulation materials.²⁹ Besides applications in industry, calcium ions play crucial roles in human physiological signaling,³⁰ including neurotransmitter release³¹ and muscle contraction³² and in activation of enzymes and hormones.³³ In medical applications, calcium chloride works as infusions in pediatric patients with low cardiac output.³⁴ Because of its importance in both biological and technological contexts, calcium chloride has been subject to various theoretical^{35–37} and experimental^{38–42} studies. While calcium is the most common dications, the micro-solvation of this ion has not been precisely studied compared to monovalent ions like alkali metal ions. The main reason is that the accurate force field description of a calcium ion within classical molecular dynamics (MD) simulations is not well established due to its ionic polarizability.^{43–46} Calcium cation can strongly polarize surrounding water molecules,⁴⁷ so capturing the complex features of calcium is rather challenging in typical nonpolarizable MD simulations. One approach to handle this effect for calcium and magnesium is to distribute the charges and the van der Waals centers to multiple sites represented by dummy atoms.⁴³ Recently, it has been shown that polarization can be effectively accounted for within nonpolarizable simulations via rescaling ionic charges.⁴⁸ We make use of this latter approach in this paper for the classical force field simulations of the $\text{CaCl}_2(\text{H}_2\text{O})_n$ clusters.

Besides the requirement of the accuracy of the classical molecular force field description of calcium ion, configuration sampling of relatively large size clusters poses another challenge. Because of many local minima that may exist on the potential energy surface separated by high energy barriers, the thorough sampling of the configuration space of the clusters is difficult. In the current study, we used integrated tempering sampling (ITS) molecular dynamics⁴⁹ to increase the sampling efficiency and to search for structures with low potential energies.

In this article, we combine photoelectron spectroscopy with computations in which both the classical force field and *ab initio* methods are applied to study calcium chloride. This paper is organized as follows: in Sec. II, we describe the details of the mass selected anion photoelectron spectroscopy experiments. Then we illustrate the approach for effectively accounting for polarization effects via ionic charge rescaling. Finally, we briefly introduce the integrated tempering sampling (ITS) sampling method and the details of the *ab initio* calculations. The results of photoelectron spectroscopy of $\text{CaCl}_2(\text{H}_2\text{O})_n^-$ are presented in Sec. III, which are then compared to theoretical results. In Sec. IV, we examine the structure of typical anion clusters and their neutral counterparts and discuss the evolution of Ca–Cl distances in $\text{CaCl}_2(\text{H}_2\text{O})_n$ clusters as the cluster size increases.

II. EXPERIMENTAL AND THEORETICAL METHODOLOGIES

A. Experimental methods

Experiments were conducted on a home-made apparatus consisting of a laser vaporization source, a time-of-flight mass spectrometer, and a magnetic-bottle photoelectron spectrometer, as described elsewhere.²¹ $\text{CaCl}_2(\text{H}_2\text{O})_n^-$ clusters were generated in the laser vaporization source, in which a rotating and translating CaCl_2 target was ablated with second harmonic (532 nm) light pulses from a nanosecond Nd:YAG laser (Continuum Surelite II-10). Helium carrier gas at ~ 0.4 MPa backing pressure seeded with water vapor was allowed to expand through a pulsed valve to provide water molecules for the formation of $\text{CaCl}_2(\text{H}_2\text{O})_n^-$ clusters. The formed clusters were mass-analyzed using time-of-flight mass spectrometry. The most abundant isotopologues in the $\text{CaCl}_2(\text{H}_2\text{O})_{0-8}^-$ clusters were mass-selected and decelerated before being photodetached by photons at 532 nm from another nanosecond Nd:YAG laser (Continuum Surelite II-10). The resulting electrons were energy-analyzed using the magnetic-bottle photoelectron spectrometer. The photoelectron spectra were calibrated with the spectra of Cs^- and Bi^- taken under similar conditions. Typical instrumental resolution was ~ 40 meV for electrons with kinetic energies of 1 eV.

B. Theoretical methodology and simulation details

Briefly, it has been shown that polarization can be effectively accounted for within nonpolarizable simulations via rescaling ionic charges by multiplying atomic partial charges by a coefficient and, at the same time, readjusting the van der Waals parameters.^{48,50,51} This method is called electronic continuum correction with rescaling (ECCR) which leads to significant improvements in the description of calcium ions. In this study, we used the charge rescaled force field developed by Jungwirth *et al.*,⁵² in which they provided a calcium model that could be reliably used in simulations of aqueous solutions of calcium ions in various aqueous and biological applications.^{53,54} The force field format we used is based on a pairwise additive potential that includes a Coulombic treatment of electrostatic interaction and a Lennard-Jones (LJ) representation of van der Waals interaction. In this formulation, the potential energy (E_{ij}) between any pair of non-bonded atoms (i and j) in a system composed of ions and water molecules is usually expressed as the sum of the van der Waals interaction energy E_{vdw} and the Coulombic interaction energy $E_{Coulombic}$, namely,

$$E_{ij} = 4\epsilon_{ij} \left[\left(\frac{\sigma_{ij}}{r_{ij}} \right)^{12} - \left(\frac{\sigma_{ij}}{r_{ij}} \right)^6 \right] + \lambda_i \lambda_j \frac{q_i q_j}{4\pi \epsilon_0 r_{ij}}.$$

In the above equation, r_{ij} is the distance between the two atoms; q_i and q_j are the point charges of the atoms; ϵ_0 is the permittivity of vacuum; λ_i and λ_j describe the Coulombic polarizable effect of atoms; and σ_{ij} and ϵ_{ij} are the distance at which the inter-particle potential is zero and the well depth of the LJ potential, respectively. Lorentz–Berthelot combination rules⁵⁵ were used to describe the van der Waals interaction between

two different kinds of atoms. The force field parameters are taken from the previous description of calcium.⁵²

Integrated tempering sampling (ITS) molecular dynamics simulation using the AMBER12 suite of program⁵⁶ was performed for each of $\text{CaCl}_2(\text{H}_2\text{O})_n^{-/0}$ ($n = 0-8$) clusters. Hundreds of different low-energy configurations were obtained from the 100 ns-long simulated trajectories. The sampled structures were then optimized using the steepest descent and the conjugate gradient algorithms. After molecular dynamics calculations using the ECCR force field, optimized low-energy structures of $\text{CaCl}_2(\text{H}_2\text{O})_n^{-/0}$ ($n = 0-8$) clusters and their neutral counterparts were re-optimized with density functional theory employing the ωB97XD functional⁵⁷ implemented in the Gaussian09 program package. Pople-type basis set 6-311++G(d,p)⁵⁸ was used for all atoms. For all clusters, the harmonic frequencies were calculated to confirm that the obtained structures are real local minima and to estimate the zero-point vibrational energies. Finally the single point energies of the anionic and neutral clusters with $n = 0-8$ were also calculated by employing coupled-cluster theory, including single, double, and non-iterative triple excitations [CCSD(T)]⁵⁹ based on structures optimized at the $\omega\text{B97XD}/6-311++\text{G}(\text{d},\text{p})$ level. Natural population analysis (NPA) was performed.⁶⁰

III. EXPERIMENTAL RESULTS

The photoelectron spectra of $\text{CaCl}_2(\text{H}_2\text{O})_n^{-/0}$ ($n = 0-8$) clusters were recorded with photons at 532 nm, as shown in Fig. 1. The vertical detachment energies (VDEs) of these clusters were measured from the peak apex of the corresponding spectrum, while adiabatic detachment energies (ADEs) were estimated by adding the instrument resolution to the electron binding energy (EBE) at the crossing point of the leading edges of the first peak and baseline. The VDEs and

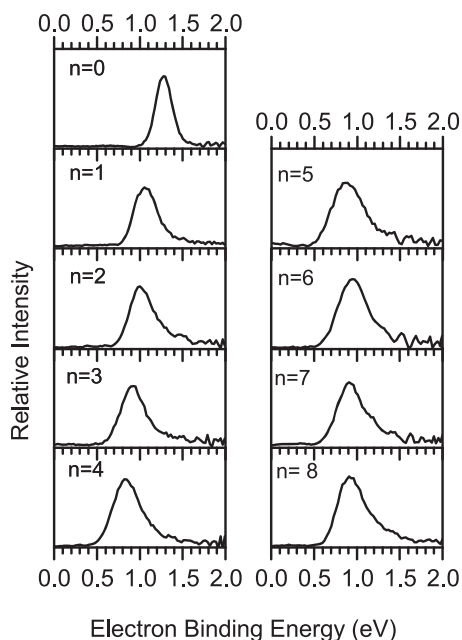


FIG. 1. Photoelectron spectra of $\text{CaCl}_2(\text{H}_2\text{O})_n^{-/0}$ ($n = 0-8$) recorded with 532 nm photons.

TABLE I. Low energy isomers of $\text{CaCl}_2(\text{H}_2\text{O})_n^{-/0}$ ($n = 0-8$) and a comparison of theoretical VDEs and ADEs with experimental values. ΔE , VDE, and ADE were obtained at the CCSD(T)// $\omega\text{B97XD}/6-311++\text{G}(\text{d},\text{p})$ level, and ΔE and ADE were corrected using zero-point energies calculated at the $\omega\text{B97XD}/6-311++\text{G}(\text{d},\text{p})$ level. The uncertainties of the experimental VDEs and ADEs are ± 0.08 eV.

n	Isomer	ΔE (eV)	Theoretical		Experimental	
			VDE (eV)	ADE (eV)	VDE (eV)	ADE (eV)
0	0a	0.000	1.35	1.12	1.28	1.08
1	1a	0.000	0.84	0.71	1.06	0.80
	1b	0.007	1.22	0.70		
	1c	0.182	1.73	0.52		
2	2a	0.000	0.96	0.56	0.98	0.64
	2b	0.033	1.00	0.53		
	2c	0.092	0.72	0.47		
3	3a	0.000	0.95	0.28	0.92	0.58
	3b	0.058	0.63	0.35		
	3c	0.128	0.80	0.21		
	3d	0.203	1.00	0.35		
4	4a	0.000	0.82	0.40	0.84	0.50
	4b	0.009	0.92	0.31		
	4c	0.047	0.78	0.20		
	4d	0.064	0.83	0.44		
5	5a	0.000	0.94	0.94	0.87	0.50
	5b	0.013	1.03	0.71		
	5c	0.018	0.78	0.32		
	5d	0.018	0.71	0.78		
6	6a	0.000	0.85	0.39	0.96	0.52
	6b	0.017	0.89	0.37		
	6c	0.048	1.09	0.44		
	6d	0.052	1.08	0.49		
7	7a	0.000	0.94	0.38	0.91	0.64
	7b	0.005	0.98	0.35		
	7c	0.043	1.09	0.41		
	7d	0.048	1.31	0.50		
8	8a	0.000	1.14	0.38	0.93	0.60
	8b	0.012	0.95	0.39		
	8c	0.013	1.04	0.56		
	8d	0.076	0.93	0.50		

ADEs determined are summarized in Table I. Each spectrum shows only one dominant broad peak. When the number of water molecules equals 0–4, the main peaks in the spectra of $\text{CaCl}_2(\text{H}_2\text{O})_n^{-/0}$ shift steadily from 1.30 eV to 0.84 eV, decreasing with the addition of every single water molecule to the cluster. Then, the peak position increases slightly from 0.84 eV to 0.93 eV when the number of water molecules increases from 4 to 8.

IV. THEORETICAL RESULTS AND DISCUSSION

We found a rather large number of low-lying isomers of $\text{CaCl}_2(\text{H}_2\text{O})_n^{-/0}$ clusters by theoretical calculations, which is consistent with the broad photoelectron spectral features of these clusters observed in the experiments, as multiple isomers might contribute to the experimental spectra. Typical low-lying energy isomers of $\text{CaCl}_2(\text{H}_2\text{O})_n^{-/0}$ ($n = 0-5$) clusters and their neutral counterparts are shown in Figs. 2 and 3, respectively. The calculated relative energies, VDEs, and ADEs of $\text{CaCl}_2(\text{H}_2\text{O})_n^{-/0}$ ($n = 0-8$) are listed in Table I,

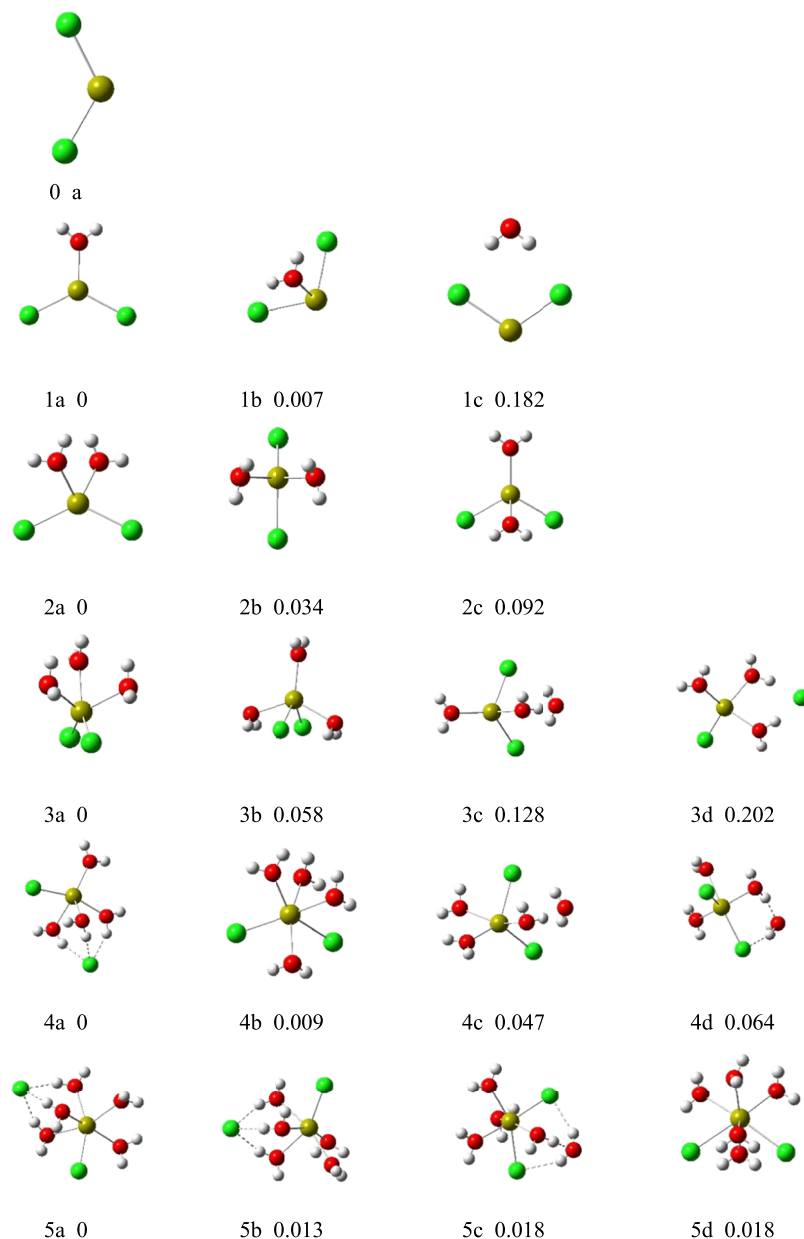


FIG. 2. Typical low-lying isomers of $\text{CaCl}_2(\text{H}_2\text{O})_n^-$ ($n = 0-5$). The relative energies were calculated at the CCSD(T)// $\omega\text{B97XD}/6-311++\text{G}(\text{d},\text{p})$ level of theory and are corrected by the zero point energies calculated at the $\omega\text{B97XD}/6-311++\text{G}(\text{d},\text{p})$ level. The yellow and green balls stand for the Ca and Cl atoms, respectively.

along with experimental VDEs and ADEs for comparison. The table shows that the theoretical VDEs of the most stable isomers of $\text{CaCl}_2(\text{H}_2\text{O})_n^-$ are in reasonable agreement with the experimental values, indicating that these isomers, found by theoretical calculations, are likely the ones detected in the experiments. In the following discussions, we examined the structures of $\text{CaCl}_2(\text{H}_2\text{O})_n^-$ and their corresponding neutral counterparts in more detail in order to reveal their structural evolution with the increase of the number of water molecules.

As shown in Fig. 2, bare CaCl_2^- anion (0a) has a bent structure with the $\angle\text{ClCaCl}$ angle of 123° and Ca—Cl bond lengths of about 2.56 Å. The theoretical VDE of CaCl_2^- anion (1.35 eV) is in good agreement with the experimental value (1.30 eV). Unlike the bent structure of CaCl_2^- anion, neutral CaCl_2 (0a' in Fig. 3) has an almost linear structure with $\angle\text{ClCaCl} = 173^\circ$ and Ca—Cl bond lengths of 2.47 Å. Namely, the $\angle\text{ClCaCl}$ angle in neutral CaCl_2 is larger

and the Ca—Cl bonds are shorter than those in the corresponding anion. Similar features are observed in the larger clusters.

Three low-lying isomers for $\text{CaCl}_2(\text{H}_2\text{O})^-$ were obtained from the structure optimization, and the structures are shown in Fig. 2, in which H_2O and CaCl_2^- are arranged to be head-to-head (1a), parallel (1b), and tail-to-tail (1c), respectively. Isomer 1a has a head-to-head quasi-planar structure formed by H_2O and CaCl_2^- via the Ca—O interaction. In isomer 1b, H_2O connects to CaCl_2^- via one Ca—O interaction and two $\text{OH}\cdots\text{Cl}$ hydrogen bonds, in which the HOH plane is parallel to the ClCaCl plane. Isomer 1c has a planar structure with H_2O and CaCl_2^- interacting through two $\text{OH}\cdots\text{Cl}$ hydrogen bonds, which is in reverse to 1a and forms a tail-to-tail structure. The $\angle\text{ClCaCl}$ angles in isomer 1a, 1b, and 1c are 125° , 112° , and 111° , respectively. In addition, isomers 1b and 1c are higher in energy than 1a by 0.007 and 0.182 eV, respectively. As for the neutral $\text{CaCl}_2(\text{H}_2\text{O})$, after optimization, all initial structures

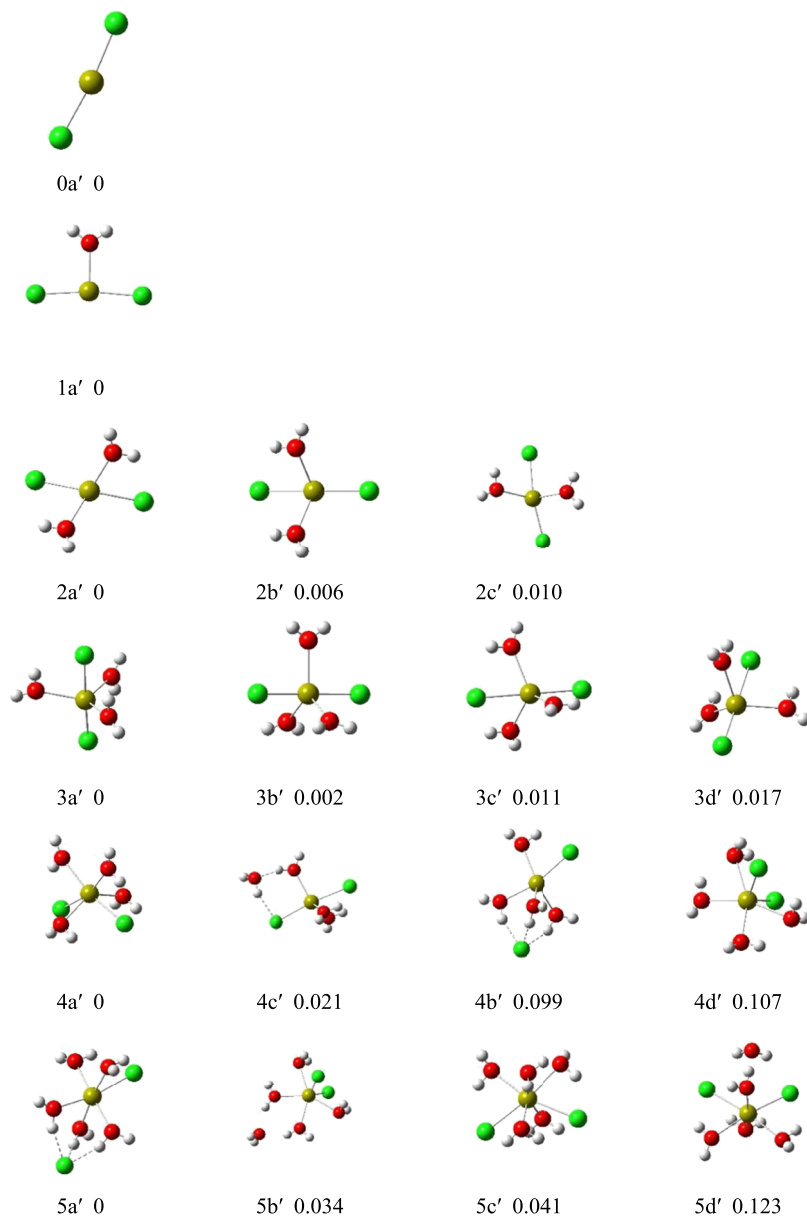


FIG. 3. Typical low-lying isomers of $\text{CaCl}_2(\text{H}_2\text{O})_n$ ($n = 0-5$). The relative energies were calculated at the CCSD(T)// $\omega\text{B97XD}/6-311++\text{G}-(\text{d},\text{p})$ level of theory and are corrected by the zero point energies calculated at the $\omega\text{B97XD}/6-311++\text{G}-(\text{d},\text{p})$ level. The yellow and green balls stand for the Ca and Cl atoms, respectively.

converge to the head-to-head structure with the oxygen atom of H_2O interacting with the Ca ion (1a'). A larger $\angle\text{ClCaCl}$ angle of 172° than that of the anionic counterpart is found. As shown in Table II, both of the Ca—Cl bond lengths are 2.51 \AA . Compared to the anionic counterpart, the $\text{CaCl}_2(\text{H}_2\text{O})$ cluster has a much larger $\angle\text{ClCaCl}$ angle and shorter Ca—Cl bond lengths.

We calculated the VDEs of $\text{CaCl}_2(\text{H}_2\text{O})_n^-$ ($n = 2-8$) and found that the most stable isomers' VDEs are all in good agreement with the experimental values (Table I). The $\angle\text{ClCaCl}$ angles in isomers 2a and 3a are 127° and 125° , respectively, which are similar to those in $\text{CaCl}_2(\text{H}_2\text{O})^-$ (1a). These similarities allow us to speculate the possible pathway of the structure evolution. It can be seen from Fig. 2 that the most stable isomer of $\text{CaCl}_2(\text{H}_2\text{O})_2^-$ (2a) can be derived from isomer 1a. Isomer 2a has two water molecules connected to the Ca ion via their O atoms which along with the two chlorine ions form a tetra-coordinated structure. Isomer $\text{CaCl}_2(\text{H}_2\text{O})_3^-$ (3a) can be derived from isomer 2a, with the third H_2O connected to

the Ca ion via an $\text{O}\cdots\text{Ca}$ interaction. In isomer 3a, the three water molecules are on the opposite sides of the two chloride ions. Nevertheless, in isomer 3b, two water molecules reside

TABLE II. The Ca—Cl distances (\AA) in the most stable isomers of anionic and neutral $\text{CaCl}_2(\text{H}_2\text{O})_n$ ($n = 0-8$) clusters.

n	Anion		Neutral	
	Ca—Cl (1)	Ca—Cl (2)	Ca—Cl (1)	Ca—Cl (2)
0	2.56	2.56	2.47	2.47
1	2.54	2.54	2.51	2.51
2	2.57	2.57	2.55	2.55
3	2.67	2.58	2.66	2.57
4	2.61	3.98	2.68	2.68
5	2.67	4.04	2.66	3.84
6	2.71	4.05	2.65	3.89
7	4.24	3.97	2.76	3.85
8	4.11	4.44	2.76	4.11

on the same side with the chloride ions. In the higher energy isomer 3d, one Ca—Cl ion pair is found to be separated by two water molecules. This kind of solvent-separated ionic pair was not found in $\text{MgCl}_2(\text{H}_2\text{O})_3^-$.⁶¹ In the most stable isomer of $\text{CaCl}_2(\text{H}_2\text{O})_4^-$ (4a), the angle $\angle\text{ClCaCl}$ is changed to 111° which is not close to 2a or 3a. Through distance analysis, we find that four water molecules are coordinated to the Ca ion through O atoms, and three water molecules among them insert into one of the Ca—Cl bond forming three $\text{OH}\cdots\text{Cl}$ hydrogen bonds. Therefore, one SSIP is found in the higher energy state of $\text{CaCl}_2(\text{H}_2\text{O})_3^-$, whereas in $\text{CaCl}_2(\text{H}_2\text{O})_4^-$ SSIP is present in the most stable configuration.

The most stable isomer of $\text{CaCl}_2(\text{H}_2\text{O})_5^-$ (5a) can be derived from isomer 4a, with one more water molecule interacting with the Ca ion. It has five water molecules coordinated with the Ca ion via O atoms, of which three insert into a Ca—Cl bond to form $\text{OH}\cdots\text{Cl}$ hydrogen bonds. Therefore, one Ca—Cl bond is broken in the low-lying isomers of $\text{CaCl}_2(\text{H}_2\text{O})_5^-$. To better understand the microscopic hydration of CaCl_2 , we also calculated the structures of $\text{CaCl}_2(\text{H}_2\text{O})_n^-$ ($n = 6-8$). As shown in Fig. 4, the most stable isomer of $\text{CaCl}_2(\text{H}_2\text{O})_6^-$ has one SSIP and one CIP, whereas the most stable structure of $\text{CaCl}_2(\text{H}_2\text{O})_7^-$ possesses two SSIPs with the Ca ion fully coordinated by six water molecules and the seventh water molecule staying in the second hydration shell. One Ca—Cl bond distance in $\text{CaCl}_2(\text{H}_2\text{O})_7^-$ is elongated by the solvent, and the other Ca—Cl is elongated even further. Similar to $\text{CaCl}_2(\text{H}_2\text{O})_7^-$, isomers with CIP in $\text{CaCl}_2(\text{H}_2\text{O})_8^-$ have higher energies and the low-lying isomer has two SSIPs, with each Ca—Cl bond separated by three water molecules.

The neutral clusters show very different structures. In the most stable isomer of $\text{CaCl}_2(\text{H}_2\text{O})_5$ (5a' in Fig. 3), one Ca—Cl bond is separated by three water molecules and three O atoms interact with the Cl ion via hydrogen bonds. The other Ca—Cl remains as a contact ionic pair. For $n = 6-8$, one Ca—Cl bond is separated by water molecules, while the other remains in the form of a contact ionic pair (Fig. 5). In summary, no Ca—Cl

bond is broken in the neutral $\text{CaCl}_2(\text{H}_2\text{O})_n$ clusters of $n \leq 4$ and Ca—Cl starts to form solvent separated ionic pair when $n = 5$.

In Table II, we summarize the results of distance analysis. It shows variations of Ca—Cl distances in the most stable isomers of $\text{CaCl}_2(\text{H}_2\text{O})_n^-$ ($n = 0-8$) clusters and their neutral counterparts. In the $\text{CaCl}_2(\text{H}_2\text{O})_n^-$ anion, the Ca—Cl bond distances decrease slightly from 2.56 to 2.54 Å when n increases from 0 to 1 because the excess electron is delocalized to the water molecule, which enhances the Coulombic attraction between Ca^{2+} and Cl^- ions. The Ca—Cl bond distances then increase at $n = 2$ and 3. For $n = 4-6$, one of the Ca—Cl bonds is broken, resulting in their corresponding Ca—Cl distances increased significantly to 3.98, 4.04, and 4.05 Å, respectively. When $n = 7$, the two Ca—Cl distances increase to 3.97 and 4.24 Å due to the breaking of the two Ca—Cl bonds. The two Ca—Cl distances in $\text{CaCl}_2(\text{H}_2\text{O})_8^-$ increase slightly to 4.11 and 4.44 Å compared with those of $n = 7$. For the neutral $\text{CaCl}_2(\text{H}_2\text{O})_n$ clusters, the Ca—Cl distances increase slightly from 2.47 to 2.68 Å with the increasing number of water molecules from 0 to 4; then, when $n = 5$, one of the Ca—Cl distances is elongated to 3.84 Å, while the other Ca—Cl bond length is slightly decreased to 2.66 Å. This observation is the consequence of the forming of SSIP.

So far, our structural results are energy based to include the entropic effect. We calculated harmonic vibrational frequencies and obtained the Gibbs free energies at 298 K after the optimization. For $\text{CaCl}_2(\text{H}_2\text{O})_n^-$ ($n = 0-8$) clusters, we checked the order by Gibbs free energies as well as by electronic energies. In most cases, structures with the lowest electronic energies also have the lowest Gibbs free energies, such as $\text{CaCl}_2(\text{H}_2\text{O})_n^-$ ($n = 0-4$ and $6-7$) clusters.²⁴ In another perspective, the broad features observed in the spectra indicate that multiple isomers may coexist in the experiments. For example, when $n = 1$, 1a and 1b isomers nearly degenerate in energy. Furthermore, the experimental VDE peak is located nearly at the average of two theoretical values. So we

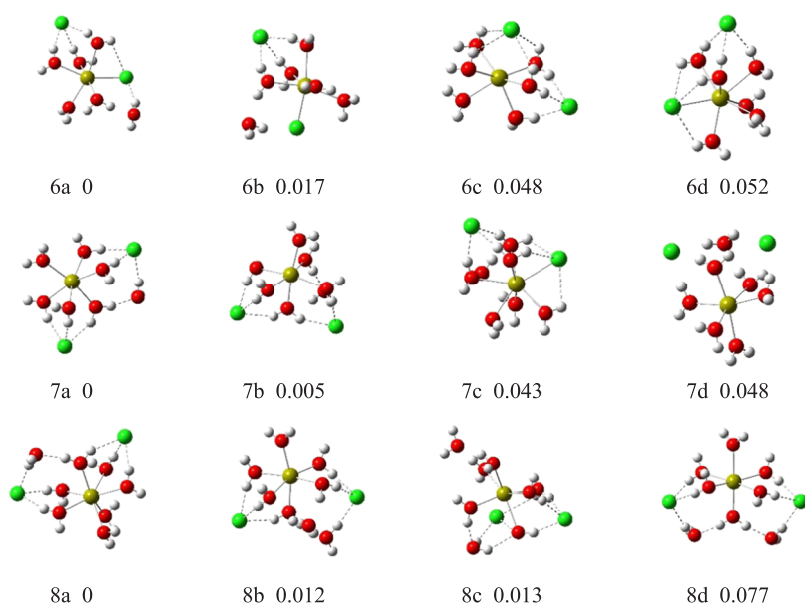


FIG. 4. Typical low-lying isomers of $\text{CaCl}_2(\text{H}_2\text{O})_n^-$ ($n = 6-8$). The relative energies were calculated at the CCSD(T)// $\omega\text{B97XD}/6-311++\text{G}(\text{d},\text{p})$ level of theory and are corrected by the zero point energies calculated at the $\omega\text{B97XD}/6-311++\text{G}(\text{d},\text{p})$ level. The yellow and green balls stand for the Ca and Cl atoms, respectively.

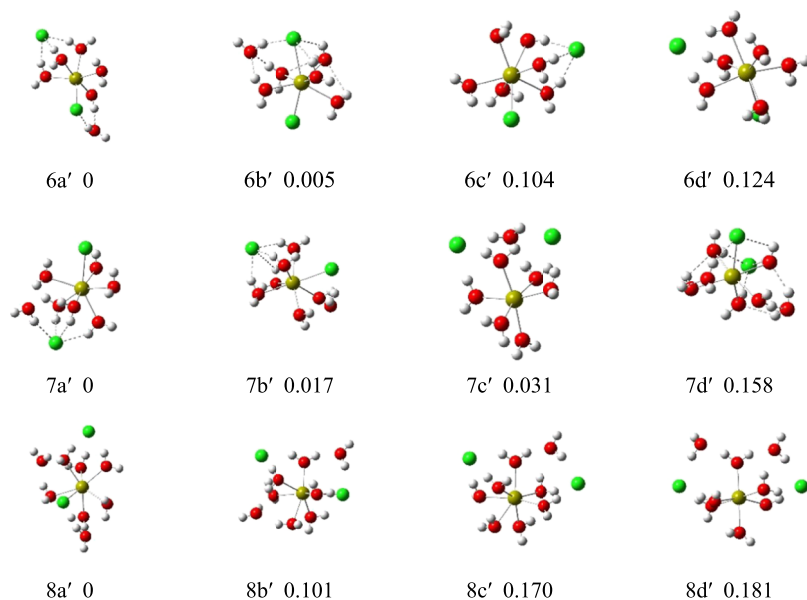


FIG. 5. Typical low-lying isomers of $\text{CaCl}_2(\text{H}_2\text{O})_n$ ($n = 6-8$). The relative energies were calculated at the CCSD(T)// $\omega\text{B97XD}/6-311++\text{G}(\text{d,p})$ level of theory and are corrected by the zero point energies calculated at the $\omega\text{B97XD}/6-311++\text{G}(\text{d,p})$ level. The yellow and green balls stand for the Ca and Cl atoms, respectively.

speculate that the broad peak observed in the spectra is actually combined with two small peaks, which means that two isomers both contribute and coexist. Similarly, when $n = 4, 5, 6,$ and 7 , energy degeneration can be explained for the broad feature of experimental spectra. We find that 5a-5d isomers nearly degenerate in energy, and the relatively low energy barrier can be overcome and isomers can coexist. As for $\text{CaCl}_2(\text{H}_2\text{O})_8^-$, the theoretical VDE of the lowest energy isomer (1.14 eV) is higher than the experimental value of 0.93 eV. It suggests that structure 8a is likely not the structure dominated in the experiments. By examining the Gibbs free energies of structures with eight water molecules, it is found that structures 8b and 8d have lower Gibbs free energy and their theoretical VDE is more consistent with the experimental measurement. We assume that 8b and 8d are likely the experimental observed structures. The entropic effect starts to dominate when the cluster size increases. For $n = 8$, although the order may differ by energy or free energy, ion pair formation remains unchanged.

To compare the charge state of the anion and neutral cluster, natural population analysis (NPA) on the charge distributions of the most stable structures for anionic and neutral $\text{CaCl}_2(\text{H}_2\text{O})_{0-8}$ clusters (Fig. 6) was performed. The charge on the Ca atom in CaCl_2^- is $+0.71 e$ which is much smaller than that in neutral CaCl_2 ($+1.62 e$), indicating that the excess electrons in CaCl_2 are mainly localized on the Ca atom. Upon addition of the first H_2O molecule, the charge on the Ca atom in $\text{CaCl}_2(\text{H}_2\text{O})^-$ increases dramatically to $+1.27 e$, with the H_2O molecule carrying a charge of $-0.63 e$. Similarly, the charges on the Ca atom of $\text{CaCl}_2(\text{H}_2\text{O})_{2-8}^-$ are in the range of $+1.22$ to $+1.36 e$ and their water molecules carry negative charges in the range of -0.56 to $-0.71 e$. In the neutral $\text{CaCl}_2(\text{H}_2\text{O})_{1-8}$ clusters, the charges on the Ca atom range from $+1.35$ to $+1.53 e$ and the water molecules carry positive charges ranging from $+0.08$ to $+0.23 e$. Therefore, the Ca atom retains its charge state in both anionic and neutral clusters, whereas variations in charge between the anionic and neutral states of $\text{CaCl}_2(\text{H}_2\text{O})_n$ clusters are mainly presented in the water molecules.

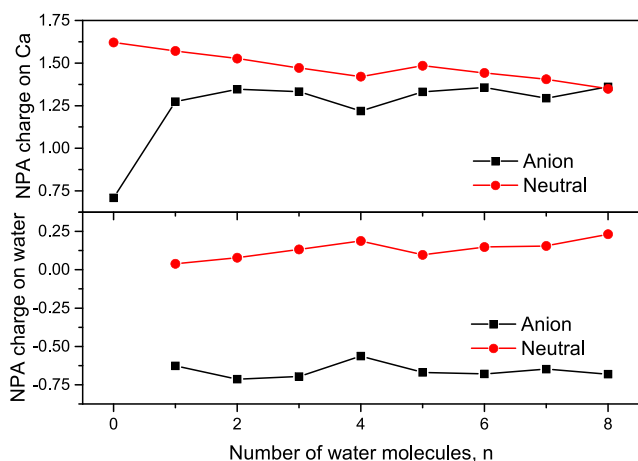


FIG. 6. NPA charge distributions on the Ca atom and water molecules in the most stable structures of anionic and neutral $\text{CaCl}_2(\text{H}_2\text{O})_n$ ($n = 0-8$) clusters.

V. CONCLUSIONS

We studied the $\text{CaCl}_2(\text{H}_2\text{O})_n^-$ clusters using size-selected anion photoelectron spectroscopy. The newly developed ECCR force field and integrated tempering enhanced sampling method were employed to obtain the structures of these clusters and their neutral counterparts. We used *ab initio* calculations to refine the detailed structures of clusters and calculated their VDEs. The most probable structures of $\text{CaCl}_2(\text{H}_2\text{O})_n^-$ clusters are determined by comparison of their theoretical VDEs to the experimental values. To understand micro-solvation process, we analyzed the changes of the ionic interactions and distances as more water molecules were introduced to the clusters. Our study showed that the solvent-separated ion pair emerges when $n = 4$ and the breaking of both Ca—Cl bonds occurs at $n = 7$ for $\text{CaCl}_2(\text{H}_2\text{O})_n^-$ anion clusters. For the neutral $\text{CaCl}_2(\text{H}_2\text{O})_n$ clusters, 5 water molecules are needed to separate the first

Ca—Cl ionic bond and this trend is consistent with our previous studies; separating the ion pair in anion clusters is easier than in neutral clusters due to the excess electron weakening the Coulombic attraction of the metal–halogen ion pair. In comparison to our solvation study of magnesium chloride, the breaking of a Ca—Cl ion pair needs fewer water molecules in neutral clusters than that of a Mg—Cl ion pair.⁶¹ Separating the first metal-Cl ion pair needs 5 and 7 water molecules for neutral $\text{CaCl}_2(\text{H}_2\text{O})_n$ and $\text{MgCl}_2(\text{H}_2\text{O})_n$ clusters, respectively, which is in coincidental agreement with the bulk solubility of CaCl_2 and MgCl_2 at ambient temperature (the solubility of CaCl_2 in water at 293 K is 1.2 times to that of MgCl_2).⁶² Our studies of calcium and magnesium chlorides clarify microsolvation at the atomic level and have a consistent trend with salt solubility. Finally, *ab initio* molecular dynamics provide another reliable route toward structural predictions,^{63,64} so we plan to improve our results by combining *ab initio* molecular dynamics simulations with enhanced sampling methods in the future work.

ACKNOWLEDGMENTS

This work was supported by the National Key Research and Development Program of China (Grant No. 2017YFA0204702), the National Natural Science Foundation of China (Grant No. 21573006, 21403249, 21773255, and U1430237), and by the Beijing National Laboratory for Molecular Sciences. We are grateful for the computational resources provided by the TianHe II supercomputer.

- ¹Y. Q. Gao, *J. Phys. Chem. B* **116**(33), 9934–9943 (2012).
²P. Lo Nostro and B. W. Ninham, *Chem. Rev.* **112**(4), 2286–2322 (2012).
³K. D. Collins, G. W. Neilson, and J. E. Enderby, *Biophys. Chem.* **128**(2-3), 95–104 (2007).
⁴R. Buchner, S. G. Capewell, G. Hefter, and P. M. May, *J. Phys. Chem. B* **103**(7), 1185–1192 (1999).
⁵K. J. Tielrooij, N. Garcia-Araez, M. Bonn, and H. J. Bakker, *Science* **328**(5981), 1006–1009 (2010).
⁶L. Yang, Y. Fan, and Y. Q. Gao, *J. Phys. Chem. B* **115**(43), 12456–12465 (2011).
⁷X.-B. Wang, H.-K. Woo, B. Jagoda-Cwiklik, P. Jungwirth, and L.-S. Wang, *Phys. Chem. Chem. Phys.* **8**(37), 4294–4296 (2006).
⁸B. Jagoda-Cwiklik, P. Jungwirth, L. Rulisek, P. Milko, J. Roithova, J. Lemaire, P. Maitre, J. M. Ortega, and D. Schroeder, *ChemPhysChem* **8**(11), 1629–1639 (2007).
⁹J. Paterová, J. Heyda, P. Jungwirth, C. J. Shaffer, A. Révész, E. L. Zins, and D. Schröder, *J. Phys. Chem. A* **115**(25), 6813–6819 (2011).
¹⁰Y. Feng, M. Cheng, X.-Y. Kong, H.-G. Xu, and W.-J. Zheng, *Phys. Chem. Chem. Phys.* **13**(35), 15865–15872 (2011).
¹¹J. W. DePalma, P. J. Kelleher, C. J. Johnson, J. A. Fournier, and M. A. Johnson, *J. Phys. Chem. A* **119**(30), 8294–8302 (2015).
¹²Z. Zeng, G.-L. Hou, J. Song, G. Feng, H.-G. Xu, and W.-J. Zheng, *Phys. Chem. Chem. Phys.* **17**(14), 9135–9147 (2015).
¹³W.-J. Zhang, G.-L. Hou, P. Wang, H.-G. Xu, G. Feng, X.-L. Xu, and W.-J. Zheng, *J. Chem. Phys.* **143**(5), 054302 (2015).
¹⁴J. Tandy, C. Feng, A. Boatwright, G. Sarma, A. M. Sadoon, A. Shirley, N. D. Rodrigues, E. M. Cunningham, S. F. Yang, and A. M. Ellis, *J. Chem. Phys.* **144**(12), 121103 (2016).
¹⁵L. Jiang, T. Wende, R. Bergmann, G. Meijer, and K. R. Asmis, *J. Am. Chem. Soc.* **132**(21), 7398–7404 (2010).
¹⁶J. C. Rienstra-Kiracofe, G. S. Tschumper, H. F. Schaefer, S. Nandi, and G. B. Ellison, *Chem. Rev.* **102**(1), 231–282 (2002).
¹⁷C. Dedonder-Lardeux, G. Gregoire, C. Jouvot, S. Martrenchard, and D. Solgadi, *Chem. Rev.* **100**(11), 4023–4037 (2000).
¹⁸C.-W. Liu, F. Wang, L. Yang, X.-Z. Li, W.-J. Zheng, and Y. Q. Gao, *J. Phys. Chem. B* **118**(3), 743–751 (2014).
¹⁹T. Wende, N. Heine, T. I. Yacovitch, K. R. Asmis, D. M. Neumark, and L. Jiang, *Phys. Chem. Chem. Phys.* **18**(1), 267–277 (2016).
²⁰A. Mizoguchi, Y. Ohshima, and Y. Endo, *J. Chem. Phys.* **135**(6), 064307 (2011).
²¹G. Feng, G.-L. Hou, H.-G. Xu, Z. Zeng, and W.-J. Zheng, *Phys. Chem. Chem. Phys.* **17**(8), 5624–5631 (2015).
²²R.-Z. Li, C.-W. Liu, Y. Q. Gao, H. Jiang, H.-G. Xu, and W.-J. Zheng, *J. Am. Chem. Soc.* **135**(13), 5190–5199 (2013).
²³P. Jungwirth, *J. Phys. Chem. A* **104**(1), 145–148 (2000).
²⁴C.-W. Liu, G.-L. Hou, W.-J. Zheng, and Y. Q. Gao, *Theor. Chem. Acc.* **133**, 1550 (2014).
²⁵G. L. Hou, C. W. Liu, R. Z. Li, H. G. Xu, Y. Q. Gao, and W. J. Zheng, *J. Phys. Chem. Lett.* **8**(1), 13–20 (2017).
²⁶Y. Zhou, D. S. Hou, J. Y. Jiang, and P. G. Wang, *Constr. Build. Mater.* **126**, 991–1001 (2016).
²⁷M. V. Achkeeva, N. V. Romanyuk, E. A. Frolova, D. F. Kondakov, D. M. Khomyakov, and V. P. Danilov, *Theor. Found. Chem. Eng.* **49**(4), 481–484 (2015).
²⁸M. A. Andreeva, V. V. Gil, N. D. Pismenskaya, V. V. Nikonenko, L. Dammak, C. Larchet, D. Grande, and N. A. Kononenko, *J. Membr. Sci.* **540**, 183–191 (2017).
²⁹J. M. Yang and J. S. Kim, *J. Appl. Polym. Sci.* **135**(6), 45821 (2018).
³⁰D. E. Clapham, *Cell* **131**(6), 1047–1058 (2007).
³¹T. M. Perney, L. D. Hirning, S. E. Leeman, and R. J. Miller, *Proc. Natl. Acad. Sci. U. S. A.* **83**(17), 6656–6659 (1986).
³²A. G. Szentgyorgyi, *Biophys. J.* **15**(7), 707–723 (1975).
³³A. B. Parekh, *Proc. Natl. Acad. Sci. U. S. A.* **97**(24), 12933–12934 (2000).
³⁴K. Averin, C. Villa, C. D. Krawczeski, J. Pratt, E. King, J. L. Jefferies, D. P. Nelson, D. S. Cooper, T. D. Ryan, J. Sawyer, J. A. Towbin, and A. Lorts, *Pediatr. Cardiol.* **37**(3), 610–617 (2016).
³⁵T. Todorova, P. H. Huenenberger, and J. Hutter, *J. Chem. Theory Comput.* **4**(5), 779–789 (2008).
³⁶Y. Mao, Y. Du, X. Cang, J. Wang, Z. Chen, H. Yang, and H. Jiang, *J. Phys. Chem. B* **117**(3), 850–858 (2013).
³⁷T. Megyes, I. Bako, S. Balint, T. Grosz, and T. Radnai, *J. Mol. Liq.* **129**(1-2), 63–74 (2006).
³⁸F. J. Amador, P. B. Stathopoulos, M. Enomoto, and M. Ikura, *FEBS J.* **280**(21), 5456–5470 (2013).
³⁹H.-Z. He, M. Wang, D. S.-H. Chan, C.-H. Leung, X. Lin, J.-M. Lin, and D.-L. Ma, *Methods* **64**(3), 212–217 (2013).
⁴⁰V. Rodriguez, M. Rivoira, A. Marchionatti, A. Perez, and N. Tolosa de Talamoni, *Arch. Biochem. Biophys.* **540**(1-2), 19–25 (2013).
⁴¹H. Ohtaki and T. Radnai, *Chem. Rev.* **93**(3), 1157–1204 (1993).
⁴²F. Jalilehvand, D. Spangberg, P. Lindqvist-Reis, K. Hermansson, I. Persson, and M. Sandstrom, *J. Am. Chem. Soc.* **123**(3), 431–441 (2001).
⁴³A. Saxena and D. Sept, *J. Chem. Theory Comput.* **9**(8), 3538–3542 (2013).
⁴⁴C. Oostenbrink, A. Villa, A. E. Mark, and W. F. Van Gunsteren, *J. Comput. Chem.* **25**(13), 1656–1676 (2004).
⁴⁵L. X. Dang and D. E. Smith, *J. Chem. Phys.* **102**(8), 3483–3484 (1995).
⁴⁶P. Bjelkmar, P. Larsson, M. A. Cuendet, B. Hess, and E. Lindahl, *J. Chem. Theory Comput.* **6**(2), 459–466 (2010).
⁴⁷M. Pavlov, P. E. M. Siegbahn, and M. Sandstrom, *J. Phys. Chem. A* **102**(1), 219–228 (1998).
⁴⁸I. Leontyev and A. Stuchebrukhov, *Phys. Chem. Chem. Phys.* **13**(7), 2613–2626 (2011).
⁴⁹Y. Q. Gao, *J. Chem. Phys.* **128**(6), 064105 (2008).
⁵⁰P. E. Mason, E. Wernersson, and P. Jungwirth, *J. Phys. Chem. B* **116**(28), 8145–8153 (2012).
⁵¹E. Pluharova, P. E. Mason, and P. Jungwirth, *J. Phys. Chem. A* **117**(46), 11766–11773 (2013).
⁵²M. Kohagen, P. E. Mason, and P. Jungwirth, *J. Phys. Chem. B* **118**(28), 7902–7909 (2014).
⁵³M. Kohagen, M. Lepsik, and P. Jungwirth, *J. Phys. Chem. Lett.* **5**(22), 3964–3969 (2014).
⁵⁴Z. Gong and H. Sun, *J. Chem. Inf. Model.* **57**(7), 1599–1608 (2017).
⁵⁵J. P. Hansen and I. R. McDonald, *Theory of Simple Liquids*, 3rd ed. (Academic Press, 2006).
⁵⁶D. A. Case et al., AMBER version 12, <http://ambermd.org>, University of California, San Francisco, 2012.
⁵⁷J. D. Chai and M. Head-Gordon, *Phys. Chem. Chem. Phys.* **10**(44), 6615–6620 (2008).
⁵⁸R. Krishnan, J. S. Binkley, R. Seeger, and J. A. Pople, *J. Chem. Phys.* **72**(1), 650–654 (1980).

- ⁵⁹J. A. Pople, M. Headgordon, and K. Raghavachari, *J. Chem. Phys.* **87**(10), 5968–5975 (1987).
- ⁶⁰A. E. Reed, R. B. Weinstock, and F. Weinhold, *J. Chem. Phys.* **83**(2), 735–746 (1985).
- ⁶¹G. Feng, C.-W. Liu, Z. Zeng, G.-L. Hou, H.-G. Xu, and W.-J. Zheng, *Phys. Chem. Chem. Phys.* **19**(23), 15562–15569 (2017).
- ⁶²P. Pradyot, *Handbook of Inorganic Chemicals* (McGraw-Hill Companies, Inc., 2003).
- ⁶³M. I. Chaudhari, M. Soniat, and S. B. Rempe, *J. Phys. Chem. B* **119**(28), 8746–8753 (2015).
- ⁶⁴M. I. Chaudhari, S. B. Rempe, and L. R. Pratt, *J. Chem. Phys.* **147**(16), 161728 (2017).